Joint In-band Full-duplex Communication and Radar Processing

Seyed Ali Hassani, Student Member, IEEE, Barend van Liempd, Member, IEEE, André Bourdoux, Senior Member, IEEE, François Horlin, Member, IEEE, and Sofie Pollin, Senior Member, IEEE

Abstract—In-band full-duplex (IBFD) technology has the potential to not only double the communication throughput but also enable additional capabilities. The fusion of radar and communication subsystems is an excellent example of how IBFD facilitates integration of radar functionality into a communication system. Developing and analysis of a joint IBFD radar-communication (RadCom) system is at the core of this study. This system derives the range-Doppler image from the state of an adaptive filter, which already exists in a typical IBFD transceiver. Our approach is waveform-independent and reuses the RF front-end while it requires little additional digital logic. The proposed system is prototyped to assess the modem-radar coexistence in a real-world IBFD communication link budget. Employing the prototyped system, we quantify the additional required logic resources and investigate whether such a RadCom approach dictates a trade-off between the two intended functionalities. The experimental results show that the proposed solution enables a communication system to detect targets within 20 m while maintaining an IBFD link with another communication node.

Index Terms—in-band full-duplex, radar-communication (RadCom), self-interference cancellation, opportunistic radar, wireless sensing, hand/body gesture detection, WiFi sensing.

I. Introduction

DUE to the rapid growth of wireless devices and services in recent years, the frequency spectrum is becoming increasingly congested and costly. This concern has forced researchers to investigate advanced methods to get the most use out of the scarce spectrum, steering the research efforts toward accommodating multiple functionalities into one wireless device. In this regard, sharing the same frequency band and hardware resources for integrating communication and radar into one platform has attracted substantial attention. Such an approach has strong potentials in both indoor and outdoor remote wireless sensing applications. For instance, this technique enables a Wi-Fi access point to provide Internet access to the users and sense them opportunistically over the downlink signal. Such an innovative radar capability integrated into a modem is not yet standardized. However, due to the recent advances and the ease of deployment, it would not be surprising to become a part of the wireless communication standards in the near future.

In this scope, the challenge is to achieve the radar extension on top of the communication mode with minimum cost. There are advanced dual-function radar-communication (DFRC) approaches that perform opportunistic communication by employing an already existing radar aperture [1]. Simultaneous emission of radar and communication signals is presented in [2] and [3] in the form of dual- or multi-beam antenna array. For example, the authors in [4] present a time-modulated method which optimizes a time-varying weight vector to control the emission of each antenna element. There are also multiple-input multiple-output (MIMO) radar and communication schemes [5] [6] in which a subset of the antenna array is allocated to radar and the rest to communication. Many other works suggest modulation-based solutions to perform in-band radar and communication. The work in [7] makes use of ultra-wideband orthogonal frequency division multiplexing (OFDM) pulses to reconstruct the radar image. In [8], a novel method for controlling a chaotic trajectory is presented to encode the binary information. This kind of frequency modulation waveform then is used for joint radar and communication. A multi-carrier agile phased array design is also proposed in [9], where the inherent spatial and spectral randomness of this scheme allows for data communication in the form of index modulation. The authors in [10] develop and linear frequency modulation in which the radar pulse is formed by the reduced phase angle modulation that can transfer low-rate information.

Although these techniques can provide high resolution sensing for long-range applications, one can list three main problems as follows.

- Deployment of array antenna requires multiple RF front-ends that makes this approach relatively expensive. Besides, such a multi-channel system is comparatively complex compared to a traditional transceiver.
- In the DFRC solutions which are enabled by dual- and multi-beam antenna arrays, the operation direction is limited, i.e. the device cannot communicate with a terminal at the same azimuth/elevation of which the

Manuscript received ...; revised ...; accepted ... . Date of publication ...; date of current version ....

Seyed Ali Hassani and Sofie Pollin are with the Electrical Engineering, KU Leuven, 3000 Leuven, Belgium (e-mail: seyedali.hassani@kuleuven.be; sofie.pollin@esat.kuleuven.be).

Barend van Liempd and André Bourdoux are with the imec Leuven, 3001 Leuven, Belgium (e-mail: barend.vanLiempd@imec.be; andre.bourdoux@imec.be).

François Horlin is with the Universit Libre de Bruxelles, 1050 Bruxelles, Belgium (e-mail: fhorlin@ulb.ac.be).

Digital Object Identifier ...

radar is operating.

- The approaches inspired by innovative modulations cannot be assigned to an already standardized framework. For instance, the OFDM-based techniques are not applicable to a sensor network operating over ZigBee.

From a broader viewpoint, a passive bi-static radar system, which exploits scattered signals from a non-cooperative communication transmitter, could also be categorized as an opportunistic remote sensing technique. However, such an approach suffers from the over-the-air reference signal extraction, the overhead due to radar Tx-Rx synchronization, and also requires multiple receivers and often needs beam antennas [11]–[13].

Although the in-band full-duplex (IBFD) technology has a long history of being employed in continuous wave radars, there are few studies demonstrating the use of IBFD for opportunistic wireless sensing and multi-purpose communication platforms. In the spectrum efficiency point of view, IBFD interest is twofold. First, it nearly doubles the connection throughput by simultaneous transmission and reception over the same frequency channel. Second, it resolves the need for a dedicated spectrum band for environment probing as the echoes of the self-transmitted signal can be captured by the device to sense the surroundings. The key technical challenge to realize concurrent in-band transmission and reception is to overcome the high-power self-interference (SI). Typically, IBFD transceivers somewhat suppress the SI signal before sampling, avoiding saturation of the Rx chain and the analog-to-digital converter (ADC). This step enables further SI cancellation at the digital sampled baseband.

In [14] and [15], we introduced an IBFD transceiver architecture that also achieves environment sensing opportunistically. The design is prototyped in [16], where a classical correlation-based radar is deployed on top of an IBFD platform. Such a radar-communication (RadCom) system performs short-range mono-static Doppler-sensing on the sample domain, operating over the standardized waveforms, and without the complexity of the DFRC systems or the requirement of bi-static counterparts. Still, range detection is not efficiently feasible with this scheme as it demands a large number of logic resources.

In contrast with our previous works with separate radar and communication subsystems, in this paper, we present a processing scheme for joint IBFD communication and range-Doppler radar. In this IBFD RadCom system, an adaptive filter is embedded to suppress the residual SI after analog cancellation and drive a radar simultaneously. As the adaptive filter cancels the environmental reflection of the transmitted signal, it is inherently environment aware and can be readily exploited as a radar. In [17]–[19], the radar functionality is carried out in the symbol domain by leveraging the channel estimation and adaptive filters for a particular modulation. Our technique is waveform-independent and does not compromise the two functionalities, while it fully reuses the RF front-end and requires few extra logic blocks to upgrade the IBFD communication modem with range-Doppler output. These features suit the proposed RadCom system for a wide variety of opportunistic sensing applications, such as Wi-Fi sensing showcases, where multiple devices can collaborate to perform target tracking and user localization.

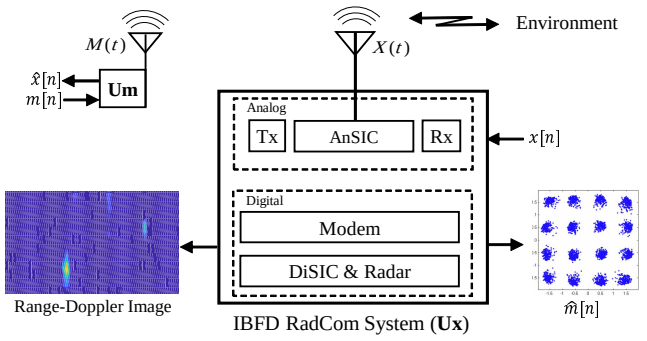

Fig. 1. Overview of the proposed IBFD RadCom system. With sharing hardware and spectrum of an IBFD communication platform, opportunistic rang-Doppler radar is possible by a minor digital block extension.

A. Contributions

Using IBFD technology in our initial work in [20], we explained how range-Doppler radar is efficiently possible. Fig. 1 illustrates the proposed RadCom system operating in a full-duplex scenario in which it forms an in-band bi-directional link with another communication terminal. As shown, the system benefits from an analog SI cancellation (AnSIC) module, which provides primary Tx-Rx isolation. The AnSIC technique in our design significantly suppresses the direct Tx leakage while it leaves no impact on the environmental reflections. This merit is achieved by employing a hybrid transformer coupled with a balance network that emulates the antenna impedance, as detailed later in Section III-A. Besides, a digital SI cancellation (DiSIC) block is deployed to suppress the residual SI signal. At the core, the DiSIC module consists of an adaptive filter that is shared between the modem and the range-Doppler radar. To the authors' knowledge, such an approach in the IBFD communication context makes this work the first of its kind.

In [20] we have already simulated the presented approach in a multi-target radar scenario. In the simulated model, an adaptive filter was included to achieve >30 dB SI rejection and detect four moving objects within 5-25 m from the RadCom system. Extending the work in [20], the key contributions of this study are summarized as follows.

- In order to give a comprehensive insight into the proposed IBFD RadCom system, the mathematical system model in our previous work in [20] is extended to describe the RF and analog baseband and the digital baseband submodels.
- In this work, we prototype the proposed IBFD RadCom design in [20] and detail the system from the implementation perspective.

- By employing the prototype, the system is extensively evaluated in a real-world IBFD communication link. We measure both communication and radar performances to investigate whether there is a trade-off between the two intended functionalities.
- Finally, we quantify the extra FPGA logic resource required on top of the IBFD communication device for implementing the proposed technique for opportunistic rang-Doppler radar.

The rest of the paper is organized as follows. Sec. II formulates the system mathematical model, incorporating the analog and digital submodels. Sec. III details the proof-of-concept prototype, which is used for the experiments in Sec. IV. Finally, Sec. V discusses few practical aspects, followed by the conclusion in Sec. VI.

II. Mathematical System Model

As shown in Fig. 1, we employ two communication entities, labeled by Ux (RadCom) and Um (remote node). The RadCom system Ux is equipped with analog and digital SI cancellation blocks and senses the environment while it sends/receives data to/from Um. This section develops a mathematical system model for the proposed IBFD RadCom system. To this end, we first describe the RF and analog bandpass model. This is further extended to the digital baseband domain, in which an adaptive filter facilitates both SI cancellation and range-Doppler radar.

A. RF and Analog Baseband

Fig. 2 depicts the analog submodel of the proposed RadCom device. This section adopts capital letters to represent the time-domain RF and analog signals whose baseband equivalents are denoted by the corresponding lowercase letters. For the sake of clarity, we develop the mathematical model in a noise-less communication scenario.

Let us define $x(t)$ as the baseband complex-valued information signal from Ux which is indicated by the bandpass communication waveform $X(t)$ after RF up-conversion,

$$X(t) = \Re\{x(t)e^{j2\pi f_c t}\}, \tag{1}$$

where, $\Re\{.\}$ denotes the real part of $\{.\}$ and f_c is the frequency of the carrier wave.

As shown in the analog model in Fig. 2, the received RF signal by Ux can be expressed in the form

$$Y(t) = R(t) + M_c(t), \tag{2}$$

where $R(t)$ (depicted by the dashed arrow in Fig. 2) is the Tx signal passed through the RF channel (including the physical environment and the AnSIC circuitry), and $M_c(t)$ denotes the desired message from Um reaching the Rx chain of the RadCom device Ux. Note that $R(t)$ involves the residual direct SI after analog suppression by the AnSIC block, and the environmental SI component reflecting off the device's surroundings.

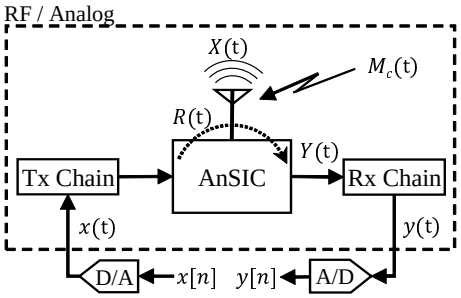

Fig. 2. System model, RF and analog baseband. In an in-band bi-directional communication link, the received signal $Y(t)$ includes the self-interference signal $R(t)$ and the transmitted message from a second party device $M_c(t)$.

Employing the multi-path channel model in [21], we define $R(t)$ in the form of time-delayed, phase- and frequency-shifted and attenuated replicas of the communication signal $x(t)$, i.e.,

$$R(t) = \Re\{\sum_{\rho} A_\rho e^{j(2\pi f_\rho t + \phi_\rho)} x(t-\tau_\rho) e^{j2\pi f_c(t-\tau_\rho)}\}, \tag{3}$$

where A_ρ, ϕ_ρ and τ_ρ denote, respectively, the attenuation, phase shift and time delay of the ρ^{th} reflection path. Besides, f_ρ is the Doppler frequency shift of the ρ^{th} reflector. Note that the contributions from the static environment and the direct Tx leakage produce echoes with a zero-frequency Doppler shift.

Similar to the transmit signal from Ux, the received intended message $M_c(t)$ can be represented as

$$M_c(t) = M(t) * H_c(t) \text{ and } M(t) = \Re\{m(t)e^{j2\pi f_c t}\}, \tag{4}$$

where $m(t)$ is the baseband complex-valued message transmitted by the remote node Um, $M(t)$ is the RF representation of $m(t)$, $H_c(t)$ characterizes the medium between Ux and Um, and $(*)$ is the time-domain convolution operator.

Finally, $y(t)$ in Fig. 2 represents the complex-valued baseband received signal after RF down-conversion. Accordingly, the complex-valued discrete-time representation of $y(t)$ after baseband sampling is

$$y[n] = y(t = \frac{n}{f_s}) \text{ and } f_s \geq B, \tag{5}$$

with n being the discrete sample integer index, f_s stands for the baseband IQ sampling frequency, and B denotes the bandwidth of the communication signal $x[n]$.

B. Digital Baseband

Fig. 3 illustrates the digital baseband joint processing model. By design, we assume that the sampling frequency is an integer (N) multiple of the communication bandwidth, i.e., $f_s = NB$.

From (2) and (5), the baseband sampled received signal is

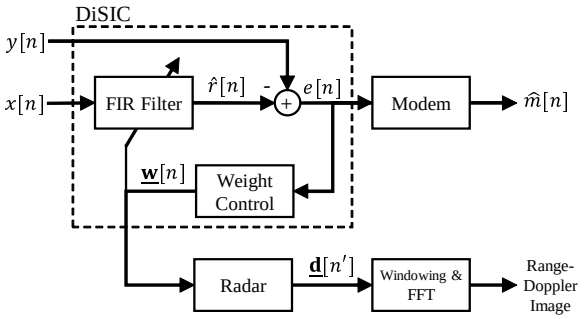

Fig. 3. Joint radar and communication digital processing. While the adaptive filter defeats the residual SI signal, the FIR filter's weights can be exploited to render a 2D rang-Doppler image.

$$y[n] = r[n] + m_c[n], \tag{6}$$

where $r[n]$ represents the SI signal $R(t)$ in the sample domain, and $m_c[n]$ denotes the baseband representation of the message from Um.

From (3), we describe $r[n]$ as

$$r[n] = \sum_{\rho} A_\rho e^{j(\mathcal{W}_\rho n + \phi_\rho)} x[n - \Delta_\rho], \tag{7}$$

where $\mathcal{W}_\rho = \frac{2\pi f_\rho}{f_s}$ denotes the Doppler frequency shift of the ρ^{th} reflector, $\Delta_\rho = \lfloor \tau_\rho f_s \rfloor$ denotes the delay of the ρ^{th} reflection path in the digital domain, and $\lfloor \{.\} \rfloor$ is the greatest integer less than or equal to $\{.\}$.

In Sec. III-A, we introduce an AnSIC scheme that can substantially suppress the direct SI signal. However, still the residual SI degrades the sensitivity of the system. Below, we explain how the DiSIC module in Fig. 3 can concurrently suppress the remaining SI and produce the radar signal.

1) Self-interference Cancellation: To enable IBFD communication, the adaptive filter reconstructs the residual SI. The estimated SI is then subtracted from the received signal $y[n]$, resulting in the error signal $e[n]$, as defined in (8).

$$e[n] = y[n] - \hat{r}[n], \tag{8}$$

where $\hat{r}[n]$ denotes the estimate of the SI signal $r[n]$, synthesized by a finite impulse response (FIR) filter, as shown in the block diagram in Fig. 3.

Imitating the communication channel, the FIR filter produces a linear combination of multiple time-delayed versions of the Tx signal in the form

$$\hat{r}[n] = \underline{\mathrm{w}}^*[n]\underline{\mathrm{x}}^{\mathrm{T}}[n], \tag{9}$$

where the superscripts * and $^{\mathrm{T}}$ denote the complex conjugate and matrix transpose, respectively. The vector $\underline{\mathrm{w}}[n]$ represents the complex-valued coefficients of the FIR filter at the discrete-time n, i.e.,

$$\underline{\mathrm{w}}[n] = [\mathrm{w}_0[n], \mathrm{w}_1[n], ..., \mathrm{w}_{Q-1}[n]], \tag{10}$$

where Q is the number of filter taps.

In addition, the reference vector $\underline{\mathrm{x}}[n]$ in (9) comprises the Q most recent samples of the Tx signal $x[n]$ as defined in (11).

$$\underline{\mathrm{x}}[n] = [\mathrm{x}[n], \mathrm{x}[n-1], ..., \mathrm{x}[n-Q-1]] \tag{11}$$

There are various adaptation techniques to tune a FIR filter [22], among which the least mean squares (LMS) algorithm reveals favorable features such as straightforward real-time implementation and sufficiently rapid convergence. This widely used method is based on gradient descent solution, where the parameters are learned by steering them to the negative direction of the gradient of the cost function, the error signal $e[n]$ in this case. Aiming a maximum SI rejection, we adapt the weights vector as

$$\underline{\mathrm{w}}[n+1] = \underline{\mathrm{w}}[n] + \mu e^*[n]\underline{\mathrm{x}}[n], \tag{12}$$

where μ is the time-independent LMS convergence factor.

Herein, we assume that the filter adaptation rate is as frequent as the baseband sample rate f_s. Note that given $x[n]$ and $m[n]$ are uncorrelated, the error signal $e[n]$ in (8) converges to $m_c[n]$ [22], so that the modem can compute $\hat{m}[n]$ as the estimate of the communication message from Um.

2) Range-Doppler Radar: From the radar point of view, the range resolution of such a system depends on the total bandwidth occupied by the communication signal $x[n]$, i.e.,

$$R_{res} = \frac{c}{2B}, \tag{13}$$

where c stands for the speed of light.

Let us define P_b as the set of reflectors located in the b^{th} radar range bin $R_b = [bR_{res}, (b+1)R_{res})$, from which the echoed SI components reach the radar within nearly an identical delay Δ_b. Accordingly, one can approximate the SI signal in (7) as a sum of the reflections from the radar range bins, as follows.

$$r[n] \approx \sum_{b} \alpha_b[n] x[n - \Delta_b], \tag{14}$$

where $\alpha_b[n]$ characterizes the overall reflected SI components from the b^{th} range bin by their amplitude, phase and frequency shifts, i.e.,

$$\alpha_b[n] = \sum_{\rho \in P_b} A_\rho e^{j(\mathcal{W}_\rho n + \phi_\rho)}. \tag{15}$$

Given the system acquires $N = f_s/B$ samples within the coherence time of the communication signal $x[n]$, from (9) and (14), one can estimate the cellwise Doppler information in (15) through N successive coefficients of the adaptive filter in the form

$$\hat{\alpha}_b[n] = \sum_{k=0}^{N-1} \mathrm{w}_{Nb+k}[n]. \tag{16}$$

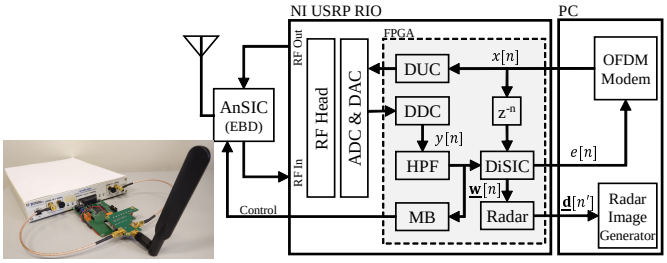

Fig. 4. The functional block diagram of the prototyped IBFD RadCom system (Right) and its picture (Left).

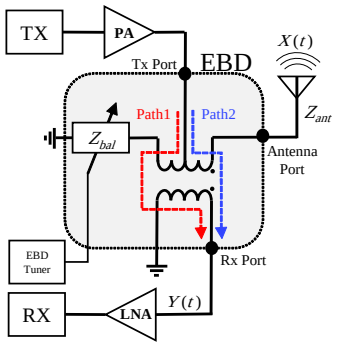

Fig. 5. Electrical balance duplexing concept. A high level of Tx-Rx isolation can be achieved by balancing the antenna's impedance Z_{ant} and the dummy load Z_{bal}.

Practically, the baseband sample rate is several times larger than the maximum Doppler frequency shift. Thus, we apply decimation to form a narrowband Doppler signal, enhancing the radar sensitivity by filtering out abrupt variations. On top of that, the radar exploits a DC-removal filter to reject the zero-frequency Dopplers, suppressing the strong impact of the residual direct TX leakage and the influence from the static environment. Hence, the radar applies filtering and downsampling to produce the non-zero Doppler information of the b^{th} range bin as

$$d_b[n'] = (\hat{\alpha}_b[n] * h[n])_{\downarrow N_d}, \tag{17}$$

where $n' = nN_d$, $h[n]$ denotes the band-pass filter, describing the low-pass and the DC-removal filters discussed above, and the operation $\{.\}_{\downarrow N_d}$ is the downsampling by a factor of N_d.

Next, the radar range-Doppler profile resulting from the proposed approach can be constructed in the form

$$\underline{\mathrm{d}}[n'] = [d_0[n'], d_1[n'], ..., d_{\lfloor \frac{Q}{N} \rfloor - 1}[n']], \tag{18}$$

where the b^{th} element of $\underline{\mathrm{d}}[n']$ approximates the Doppler information reflecting off the b^{th} radar range bin, and rates at f_s/N_d.

Finally, windowing followed by the fast Fourier transform (FFT) can be used to identify the dominant Doppler component of each range bin f_d, and consequently, calculate the radial speed of the target V, the velocity resolution V_{res} and the maximum detectable speed V_{max} as follows.

$$V = \frac{cf_d}{2f_c}\ ,\ V_{res} = \frac{cf_s}{2f_cN_dN_{fft}},\ V_{max} = \frac{cf_s}{4f_cN_d}, \tag{19}$$

where N_{fft} stands for the number of samples used to produce the FFT.

Besides, the FIR filter order Q and the processing gain N determine the maximum detectable range, i.e.,

$$R_{max} = \lfloor \frac{Q}{N} \rfloor R_{res}. \tag{20}$$

III. IBFD RadCom Prototype

In this work, we start from the simulation results in [20] and focus on prototyping, which enables experimentation in a real-life scenario. Fig. 4 (Right) depicts the functional block diagram of the proof-of-concept IBFD RadCom system whose picture is shown in Fig. 4 (Left). The prototype consists of one software-defined radio (SDR), one AnSIC module and one PC. The SDR is a NI USRP RIO with a Kintex-7 FPGA on board, allowing for real-time SI cancellation as well as radar realization. Below, this section describes the prototype in the implementation viewpoint.

A. AnSIC Module

At the core, the AnSIC employs a customized on-chip electrical-balance duplexer (EBD) [23]. As illustrated in Fig. 5, the balance between the antenna's impedance Z_{ant} and the dummy load Z_{bal} causes two equivalent copies of the transmit signal (represented by Path1 and Path2) reach the EBD's Rx port in opposite phase, leading to significant isolation between Tx and Rx ports. In this work, the dithered linear search (DLS) algorithm [24] is adopted to tune the EBD, aiming for maximum Tx-Rx isolation. The EBD adaptation is deployed on a MicroBlaze, represented by the MB block, inside the FPGA (see Fig. 4). The EBD tuning procedure has to be done regarding the antenna's near-field dynamics, for example, once at the start-up for a ceiling-mounted device. This AnSIC technique can significantly suppress the direct SI component, while leaving the environmental SI reflection untouched. This feature is essential in such a RadCom system where the environmental SI echoes have to reach the digital baseband, allowing for radar processing.

Regarding the EBD's maximum tolerable RF input and operating frequency band over which it behaves linearly, the Tx channel power in our design is limited to -5 dBm and the USRP's RF front end is tuned to 1.74 GHz. As shown in Fig. 4, the EBD antenna port is connected to an omnidirectional antenna as such the device can radiate/receive to/from all directions.

B. DiSIC Module

The prototyped system is equipped by a VHDL-based DiSIC deployed on the FPGA to allow post-analog SI cancellation. The implementation consists of a 28-tap

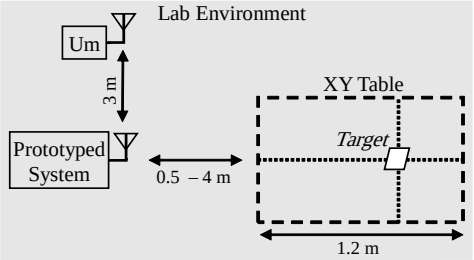

Fig. 6. Evaluation setup. While a XY positioner is involved to produce a consistent movement in each test, two communication terminals are employed in the test setup to establish an IBFD communication link.

FIR filter and a real-time LMS optimizer. The processing precision is set to 28-bit fixed-point in the proof-of-concept prototype to avoid computational issues and accelerate prototyping. Running at 80 MHz, the pipeline realization in such a design allows SI cancellation of a complex communication signal up to 40 MHz bandwidth within six clock cycles.

To accelerate the IBFD studies, we also published this VHDL-based DiSIC implementation as an opensource repository which can be cloned from [25]. This implementation allows for adaptive filters with up to 48 taps and up to 32-bit fixed-point precision.

Since the USRP digital frontend operates at 120 MHz, there are a digital up converter (DUC) and a digital down converter (DDC) to convey the baseband signal across the two clock domains (see Fig. 4). Furthermore, to avoid the USRP's DC signal at the IF baseband, the system adopts a DC-removal filter shown by the HPF in the block diagram. Moreover, there is a delay block shown by z^{-n} to compensate for the Tx baseband to Rx baseband delay. By connecting the EBD's antenna port to a 50 Ω dummy load, we measured this delay equivalent to 182 samples which is mainly dictated by the DDC and DUC in our prototype.

C. Radar Implementation

The high-speed part of the radar is also deployed on the FPGA. The weight vector $\underline{w}[n]$ in (10) is produced by the VHDL-based DiSIC and further processed by the filters and the downsampler. The parametrized realization in this part allows for an output which rates at 4.88 kHz - 308 Hz. This is implemented by a run-time configurable decimator in which the filter length is also flexible. In the next step, the range-Doppler profile $\underline{d}[n']$ in (18) is transferred to the PC by a PCI-e interface. Ultimately, by windowing (Hamming), FFT operation and 2D interpolation, the PC draws a real-time range-Doppler image.

IV. Experimental Result

By employing the prototyped platform, this section evaluates the performance of the proposed RadCom system. To this end, we first measure its SI rejection ability. The optimum system parameters are then investigated in a real-world IBFD communication scenario, followed by the radar performance analysis. As shown in Fig. 6, in addition to node Um at 3 m, there is an XY positioner in the test setup to enable identical movement in the test iterations. The devices transmit an OFDM communication signal as specified in Table I. The modem transmits communication messages at 1.74 GHz, which carries random bitstreams starting with an IEEE 802.11ac training sequence.

TABLE I
OFDM Waveform Characteristics

Parameter	Value	Parameter	Value
strength	-5 dBm	subcarriers	128 (Data+Pilot)
band	1.74 GHz	modulation	QPSK
bandwidth	5-40 MHz	ideal time	20 μs

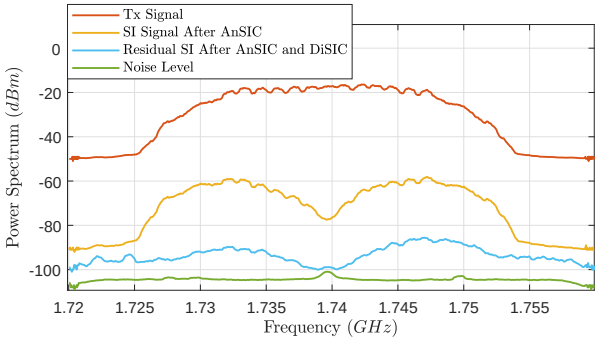

Fig. 7. Self-interference cancellation performance. -5 dBm Tx channel power, 44 dB analog SI rejection by EBD, 30 dB digital SI cancellation. Still, 24 dB further cancellation is required to push the remaining SI (-79 dBm) below the noise floor (-103 dBm), achieving the same sensitivity as the half-duplex mode.

A. SI Cancellation

Fig. 7 illustrates the power spectral densities of a 20 MHz SI signal after different stages of cancellation. This graph reveals how the joint analog and digital SI cancellation modules reduce the undesirable SI. According to this graph, the EBD resembles a notch filter. Whereas the DiSIC attenuates the residual SI uniformly over the frequency band. Table. II lists the SI rejection performance for different signal bandwidths, showing that increasing the bandwidth reduces the performance of AnSIC while the DiSIC module reveals relatively consistent performance, at -5 dBm Tx power.

B. IBFD Communication Performance

Fig. 8 shows the convergence time of the DiSIC module in a static environment where the AnSIC block provides 44 dB SI cancellation and without the interference from Um. In each test, the DiSIC is triggered until the SI reduces and converges to a certain level. Then, regardless of the ultimate SI rejection performance, the time between the trigger and the residual SI settlement is measured to estimate the convergence time. This graph reveals that, one has to increase both DiSIC tuning rate f_t and adaptation factor μ to achieve a rapid SI suppression. While

TABLE II
Self-interference Cancellation Performance

B (MHz)	AnSIC (dB)	DiSIC (dB)	Overall SIC (dB)
5	55	31	86
10	48	31	79
20	44	30	74
40	40	31	71

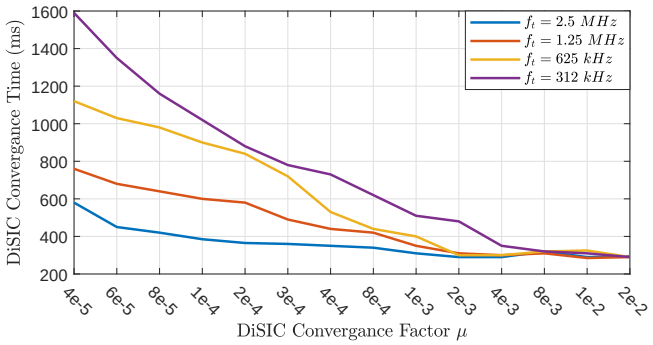

Fig. 8. DiSIC convergence time VS the adaptation factor μ as a function of the adaptive filter tuning frequency f_t in the absence of the node Um.

the DiSIC adaptation has to be fast enough to provide rapid SI rejection and track fast-moving targets, one can adjust the convergence factor μ to achieve robustness against interference and noise. To this end, we firstly define the signal-to-interference-plus-noise ratio (SINR) of the demodulated training sequence as a metric to determine the IBFD link quality, i.e.,

$$\text{SINR} = \frac{\sum_{i=0}^{N_s-1} |s[i]|^2}{\sum_{i=0}^{N_s-1} |s[i] - \hat{s}[i]|^2}, \tag{21}$$

where $s[n]$ is the training sequence of length N_s, and $\hat{s}[n]$ is its estimate calculated by the OFDM modem running on the PC (see Fig. 4).

Fig. 9 shows the measured link quality for a 20 MHz communication signal in a dynamic environment, as a function of the DiSIC adaptation factor μ. The dashed lines in this graph indicate the half-duplex performance. Note that the interval labels of the x-axis (μ) in this graph are not spaced equally. In this test, an aluminum coated plate (40 × 25 cm) moves at nearly 0.5 m/s by the XY positioner. In each iteration, the EBD is tuned once at the startup. To avoid significant environmental changes within the EBD's near-field, the plate moves at 0.5 m to 4 m away from the system under test. To assess the impact from the node Um and the distance of the target d_t, we examined the performance with four different configurations, and DiSIC tuning rate is set to be $f_t = 2.5$ MHz.

From this graph, one can find the optimum adaptation factor around $\mu = 4\text{e}{-4}$. This is obvious in this figure that the adaptation factor μ should be large enough to achieve sufficient SI cancellation and achieve a better SINR. Besides, for the case with stronger emission from Um (+5 dBm), increasing μ value significantly reduces the

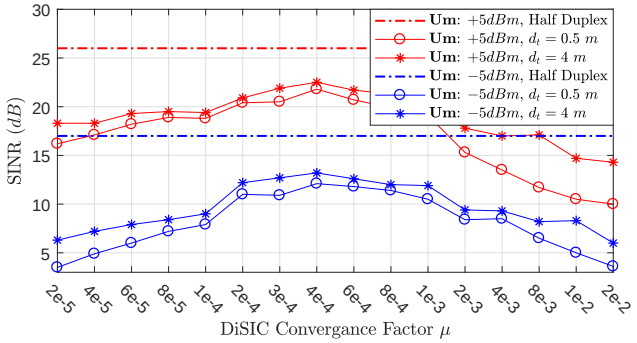

Fig. 9. Measured IBFD communication link quality in a dynamic environment where a target moves at 0.5 m/s at 0.5 m and 4 m from the prototyped RadCom system.

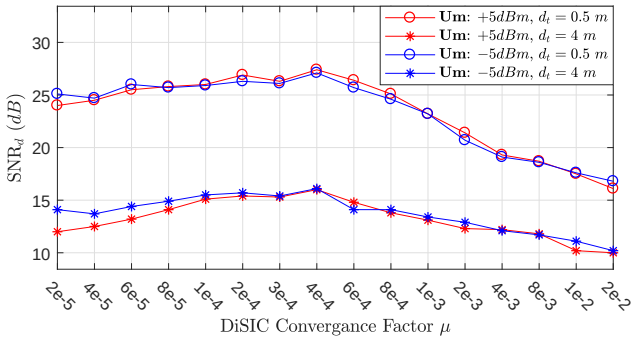

Fig. 10. Measured radar performance with the coexistence of a second party communication terminal at 3 m.

performance as it leads to instability. This is more clear when the moving plate is closer to the device. Furthermore, increasing the transmit power of Um from -5 dBm to +5 dBm, enhances the link quality by nearly 10 dB (compare the red and the blue curves at the optimum point). Moreover, we observed that nearing the target from 4 m to 0.5 m degrades the link quality slightly by 2-4 dB (compare the star curves with the ones with circles).

C. Radar Performance

This part assesses the radar performance. In this test, the target moves forward at 0.5 m/s, and in each iteration the signal-to-noise ratio (SNR) of the FFT components ($\pm 2V_{res}$) at the expected range and frequency indexes are compared to the noise level of the range-Doppler image. Fig. 10 shows the radar performance SNR_d as a function of DiSIC adaptation factor μ, when the tuning rate is set to $f_t = 2.5$ MHz. From this graph, we learn that increasing the DiSIC adaptation factor from the optimum point reduces radar performance similar to the link quality as the DiSIC becomes sensitive to interference from Um for large values of μ. We also assessed the impact of a concurrent in-band emission from Um at two different levels, -5 dBm and +5 dBm. As explained in Sec. II, the adaptive filter merely reconstructs the contribution from the SI signal and hence, an uncorrelated communication

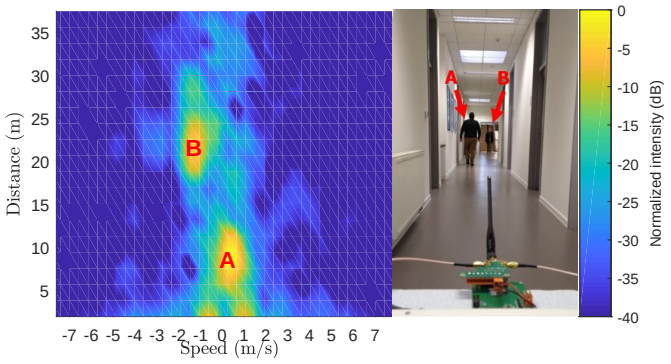

Fig. 11. Measured range-Doppler image (Left) from the experiment pictured at the Right. The prototyped RadCom system detects two human targets that walk/run away/toward the system, which emits a 40 MHz OFDM signal.

message from a second party device has nearly no impact on the radar performance (compare the red and the blue curves in Fig. 10). Moreover, we observed a better performance for the case that the plate is closer to the RadCom prototype.

In the proof-of-concept prototype, the modem is implemented on the PC side, making the communication link quality assessment inaccurate for higher bandwidths than 20 MHz by overwhelming the PC. Thus, to represent the radar capability at this point, we use a 40 MHz OFDM signal to achieve a better range resolution while we disabled the modem to relax the PC. Fig. 11 depicts the measured 2D range-Doppler image. In this test, two persons, labeled by A and B in the picture, walk away (A) and run toward (B) the prototyped system, which is placed in a corridor and emits a 40 MHz OFDM communication signal. Note that here, we skipped the sum in (16) and mapped the first 20 filter coefficients directly to the distance axis as such it improves the graphical drawing of the 2D graph. Given 80 MHz sampling rate, we calculate the maximum detectable range R_{max}=37.5 m. This experiment proves the ability of the proposed technique in this paper to detect multiple targets at different ranges and velocities.

D. RadCom FPGA Resource Usage

In addition to the communication and radar quality evaluation, it is also interesting to investigate how much extra FPGA logic is required to embed radar functionality into an IBFD communication system. Based on the prototyped system explained in Sec. III, Table III details the FPGA (Kintex-7) resources as are necessary for the IBFD communication device as well as those that are needed for the IBFD RadCom system. This table confirms that, on top of the original IBFD platform, a small set of FPGA components is adequate to effectively render the two mentioned concurrent in-band functionalities.

TABLE III
FPGA Resource Usage (Xilinx Kintex-7)

Component	Available	Communication	RadCom
Registers	508.4 k	28%	31%
DSPs	1540	72%	73%
Block RAMs	794	60%	68%
LUTs	254.2 k	52%	60%

V. Discussion

Increasing the Tx power in our proof-of-concept prototype causes non-linear SI components mainly introduced by the EBD and the power amplifier. Thus, to assess joint radar-communication performance by the prototype, we limited the Tx power to -5 dBm, avoiding nonlinearities that can impact the radar sensitivity and degrade the IBFD link severely. However, on top of the linear DiSIC in our prototype, the hardware imperfections and nonlinearities also have to be modeled prior to the adaptive filter. In [26], for instance, we proposed a Hammerstein model, with a nonlinear part modeling the transmitter nonidealities followed by a linear filter to model the SI channel. The non-linear part includes a spline-based model for the nonlinear power amplifier, a polynomial model for baseband nonlinearities, as well as models for I/Q mismatch and local oscillator leakage. In contrast with the traditionally used memory-polynomial-based non-linear models, a real-time implementation of the Hammerstein model is accompanied by comparatively lower computational complexity. Besides, it delivers a significant SI suppression performance compared to the only-linear model. This way one can achieve optimum SI suppression and improve both radar and communication.

The other disadvantageous of the EBD approach is the non-uniform SI rejection behavior, as is visible in Fig. 7. The possible solutions to overcome the EBD notch-shape response can be listed as a) using an EBD design with a broader SI suppression range, b) employing parallel EBDs, or c) modelling the EBD frequency response at the digital cancellation step.

Besides, as mentioned in Section I, the required hardware via implementing the proposed approach in this work is more efficient than the technique in [16]. The reason is two-fold: a) the approach in [16] requires several IQ mixers to obtain the Doppler information of each radar range bean while the proposed technique in this work reuses the already existing blocks from the DiSIC. b) Since the adaptive filter update rate is less than the sampling rate, the approach in this work requires partially smaller logic for decimation.

Moreover, the simulation results in Fig. 12 reveals that compared to the correlation-based Doppler radar in [16], the joint scheme proposed in this work is less sensitive to the level of the direct SI suppression by the AnSIC module. For this analysis, the simulated layout in [20] is adopted and both of the approaches above are applied to extract the Doppler signal of the nearest target. Then, the same technique in Section IV-C is used to estimate the sensing

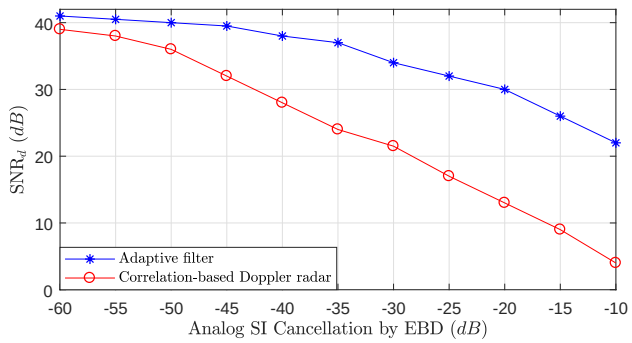

Fig. 12. Radar performance compassion between the joint scheme proposed in this paper and the correlation-based Doppler radar in [16], as a function of analog SI rejection by the EBD.

performance. The graph in Fig. 12 illustrates that reducing the direct SI cancellation degrades the correlation-based radar more than the technique with adaptive filtering. Although the reason has to be studied more analytically, the use of multiple taps and the feedback mechanism can already explain the better results with the adaptive filtering approach.

VI. Conclusion

This paper has introduced an efficient strategy to integrate a radar subsystem into an IBFD communication transceiver by joint full-duplex and radar signal processing. To achieve IBFD, the proposed system employs an analog SI cancellation module that does not impact the environmental reflections of the transmit signal. Then, an adaptive filter is embedded at the digital side to suppresses the residual SI, while the filter also projects the environmental Doppler information on its weight vector.

Using a testbed, we measured the IBFD link quality (in terms of SINR) and the radar performance. We conclude that a better SI rejection by the digital SI canceller gains radar performance. More importantly, we showed a simultaneous in-band transmission does not overwhelm the radar in a practical scenario. Nonetheless, with or without the radar block, we observed that dynamics close to the device could degrade the IBFD link quality as they impose substantial abrupt SI variation. Furthermore, we quantified a small number of additional logic blocks to perform the joint radar processing. These features enable the proposed approach to satisfy a wide variety of RadCom showcases.

References

[1] A. Hassanien, M. G. Amin, E. Aboutanios, and B. Himed, "Dual-function radar communication systems: A solution to the spectrum congestion problem," IEEE Signal Processing Magazine, vol. 36, no. 5, pp. 115–126, 2019.

[2] P. M. McCormick, S. D. Blunt, and J. G. Metcalf, "Simultaneous radar and communications emissions from a common aperture, part I: Theory," in 2017 IEEE Radar Conference (RadarConf). IEEE, 2017, pp. 1685–1690.

[3] P. M. McCormick, B. Ravenscroft, S. D. Blunt, A. J. Duly, and J. G. Metcalf, "Simultaneous radar and communication emissions from a common aperture, part II: experimentation," in 2017 IEEE Radar Conference (RadarConf). IEEE, 2017, pp. 1697–1702.

[4] J. Euziere, R. Guinvarc'h, M. Lesturgie, B. Uguen, and R. Gillard, "Dual function radar communication time-modulated array," in 2014 International Radar Conference. IEEE, 2014, pp. 1–4.

[5] F. Liu, C. Masouros, A. Li, H. Sun, and L. Hanzo, "MU-MIMO communications with MIMO radar: From co-existence to joint transmission," IEEE Transactions on Wireless Communications, vol. 17, no. 4, pp. 2755–2770, 2018.

[6] K. Singh, S. Biswas, T. Ratnarajah, and F. A. Khan, "Transceiver design and power allocation for full-duplex MIMO communication systems with spectrum sharing radar," IEEE Transactions on Cognitive Communications and Networking, vol. 4, no. 3, pp. 556–566, 2018.

[7] D. Garmatyuk, J. Schuerger, Y. Morton, K. Binns, M. Durbin, and J. Kimani, "Feasibility study of a multi-carrier dual-use imaging radar and communication system," in 2007 European Microwave Conference. IEEE, 2007, pp. 1473–1476.

[8] C. S. Pappu, T. L. Carroll, and B. C. Flores, "Simultaneous radar-communication systems using controlled chaos-based frequency modulated waveforms," IEEE Access, vol. 8, pp. 48 361–48 375, 2020.

[9] T. Huang, X. Xu, Y. Liu, N. Shlezinger, and Y. C. Eldar, "A dual-function radar communication system using index modulation," in 2019 IEEE 20th International Workshop on Signal Processing Advances in Wireless Communications (SPAWC). IEEE, 2019, pp. 1–5.

[10] M. Nowak, M. Wicks, Z. Zhang, and Z. Wu, "Co-designed radar-communication using linear frequency modulation waveform," IEEE Aerospace and Electronic Systems Magazine, vol. 31, no. 10, pp. 28–35, 2016.

[11] B. Tan, K. Woodbridge, and K. Chetty, "A real-time high resolution passive WiFi Doppler-radar and its applications," in Radar Conference (Radar), 2014 International. IEEE, 2014, pp. 1–6.

[12] W. Li, B. Tan, R. J. Piechocki, and I. Craddock, "Opportunistic physical activity monitoring via passive WiFi radar," in e-Health Networking, Applications and Services (Healthcom), 2016 IEEE 18th International Conference on. IEEE, 2016, pp. 1–6.

[13] M. A. Attalah, T. Laroussi, F. Gini, and M. S. Greco, "Range-Doppler fast block LMS algorithm for a DVB-T-based passive bistatic radar," Signal, Image and Video Processing, vol. 13, no. 1, pp. 27–34, 2019.

[14] S. A. Hassani, A. Guevara, K. Parashar, A. Bourdoux, B. van Liempd, and S. Pollin, "An in-band full-duplex transceiver for simultaneous communication and environmental sensing," in 2018 52nd Asilomar Conference on Signals, Systems, and Computers. IEEE, 2018, pp. 1389–1394.

[15] S. A. Hassani, K. Parashar, A. Bourdoux, B. van Liempd, and S. Pollin, "Doppler radar with in-band full duplex radios," in IEEE INFOCOM 2019-IEEE Conference on Computer Communications. IEEE, 2019, pp. 1945–1953.

[16] S. A. Hassani, V. Lampu, K. Parashar, L. Anttila, A. Bourdoux, B. v. Liempd, M. Valkama, F. Horlin, and S. Pollin, "In-band full-duplex radar-communication system," IEEE Systems Journal, 2020.

[17] C. Sturm and W. Wiesbeck, "Waveform design and signal processing aspects for fusion of wireless communications and radar sensing," Proceedings of the IEEE, vol. 99, no. 7, pp. 1236–1259, 2011.

[18] P. Kumari, J. Choi, N. González-Prelcic, and R. W. Heath, "IEEE 802.11 ad-based radar: An approach to joint vehicular communication-radar system," IEEE Transactions on Vehicular Technology, vol. 67, no. 4, pp. 3012–3027, 2017.

[19] C. Sturm, T. Zwick, and W. Wiesbeck, "An OFDM system concept for joint radar and communications operations," in VTC Spring 2009-IEEE 69th Vehicular Technology Conference. IEEE, 2009, pp. 1–5.

[20] S. A. Hassani, B. van Liempd, A. Bourdoux, F. Horlin, and S. Pollin, "Adaptive filter design for simultaneous in-band full-duplex communication and radar," in European Radar

Conference. The European Microwave Association (EuMA), 2020.
[21] A. Goldsmith, Wireless communications. Cambridge university press, 2005.
[22] B. Kovačević, Z. Banjac, and M. Milosavljević, Adaptive digital filters. Springer Science & Business Media, 2013.
[23] B. van Liempd, B. Hershberg, S. Ariumi, K. Raczkowski, K.-F. Bink, U. Karthaus, E. Martens, P. Wambacq, and J. Craninckx, "A +70 dBm IIP3 electrical-balance duplexer for highly integrated tunable front-ends," IEEE Transactions on Microwave Theory and Techniques, vol. 64, no. 12, pp. 4274–4286, 2016.
[24] A. C. Carusone and D. A. Johns, "Analog filter adaptation using a dithered linear search algorithm," in Circuits and Systems, 2002. ISCAS 2002. IEEE International Symposium on, vol. 4. IEEE, 2002, pp. IV–IV.
[25] KU Leuven, "VHDL-based Open Source Digital Self-interference Canceller," https://github.com/SAHassani/KU_Leuven_DiSIC.
[26] L. Anttila, V. Lampu, S. A. Hassani, P. P. Campo, D. Korpi, M. Turunen, S. Pollin, and M. Valkama, "Full-duplexing with SDR devices: Algorithms, fpga implementation and real-time results," IEEE Transactions on Wireless Communications, 2020.

Seyed Ali Hassani obtained his B.Sc. degree in electrical engineering from Arak Azad University, Arak, Iran in 2008. He then worked as an R&D engineer in the industry to gain his professional experience. In 2014, he started M.Sc. in Information Technology - Signal Processing in Finland where he graduated with distinction from Tampere University of Technology, in 2016. Currently, he is a Ph.D. researcher at KU Leuven, focusing on Context-aware Ultra-Reliable Networks. His main research interests are low-latency networks, radar signal processing, and wireless in-band full-duplex communication.

Barend van Liempd received the B.Sc. and M.Sc. degree in electrical engineering at the Eindhoven University of Technology, Eindhoven, The Netherlands, in 2009 and 2011, respectively, and the Ph.D. degree in 2017 at the Vrije Universiteit Brussel, Brussels, Belgium, in collaboration with imec, Heverlee, Belgium. His Ph.D. dissertation concerned tunable, highly integrated RF front-end circuits and modules in SOI CMOS. In 2011, he joined imec, working as an R&D Engineer on multi-standard transceivers, until 2014, when he became a Ph.D. Researcher and later a Senior Researcher in 2017. He was appointed Program Manager Radar IC's in 2018, and now leads imec's radar IC R&D activities. His research interests are analog, RF and mm-Wave circuits for wireless applications. He has authored or coauthored more than 30 papers, patents and patent applications. He was the 2019 Lewis Winner Award for Outstanding Paper at the International Solid-State Circuits Conference (ISSCC).

André Bourdoux received the M.Sc. degree in electrical engineering in 1982 from the Université Catholique de Louvain-la-Neuve, Belgium. He joined IMEC in 1998 and is Principal Member of Technical Staff in the IoT research group of IMEC. He is a system level and signal processing expert for both the mm-wave wireless communications and radar teams. He has more than 15 years of research experience in radar systems and 15 years of research experience in broadband wireless communications. He holds several patents in these fields. He is the author and co-author of over 160 publications in books and peer-reviewed journals and conferences. His research interests are in the field of advanced signal processing and machine learning for wireless physical layer and high-resolution 3D/4D radars.

François Horlin received the electrical engineering degree and the Ph.D. degree from the Universite catholique de Louvain (UCL), Louvain- la-Neuve, Belgium, in 1998 and 2002, respectively. During his studies, he specialized in the field of digital signal processing for communications. In 2002, he joined the Interuniversity Micro-Electronics Center (IMEC), Leuven, Belgium where he led the project aiming at developing a fourth-generation wireless communication system in collaboration with Samsung South Korea. In 2007, he became a Professor at the Université libre de Bruxelles (ULB), Brussels, Belgium. He is an author of a book, author of a book chapter, co-author of two patents, author or co-author of more than 200 publications in well-recognized journals and conferences.

Sofie Pollin obtained her PhD degree at KU Leuven with honors in 2006. From 2006-2008 she continued her research on wireless communication, energy-efficient networks, cross-layer design, coexistence and cognitive radio at UC Berkeley. In November 2008 she returned to imec to become a principal scientist in the green radio team. Currently, she is associate professor at the electrical engineering department at KU Leuven. Her research centers around Networked Systems that require networks that are ever more dense, heterogeneous, battery powered and spectrum constrained. Prof. Pollin is BAEF and Marie Curie fellow, and IEEE senior member.